Electronic Supplementary Material (ESI) for Nanoscale.
This journal is © The Royal Society of Chemistry 2018

# Supercritical $CO_2$-induced atomistic lubrication for water flow in a rough hydrophilic nanochannel

Tuan A. Ho[1]*, Yifeng Wang[2], Anastasia Ilgen[1], Louise J. Criscenti[1], and Craig M. Tenney[3]

[1] *Geochemistry Department, Sandia National Laboratories, Albuquerque, New Mexico 87185, USA.*

[2] *Nuclear Waste Disposal Research and Analysis Department, Sandia National Laboratories, Albuquerque, New Mexico 87185, USA.*

[3] *Nuclear Incident Response Program Department, Sandia National Laboratories, Albuquerque, New Mexico 87185, USA.*

*Corresponding author*:* taho@sandia.gov*

## Supporting Information

## Content

1. Kerogen surface construction
2. Contact angle simulation
3. Poiseuille flow simulation
4. 1D-density profile of $CO_2$ with respect to kerogen atoms
5. Lennard-Jones parameters for $CO_2$, $CH_4$, $H_2O$ and muscovite

## 1. Kerogen surface construction

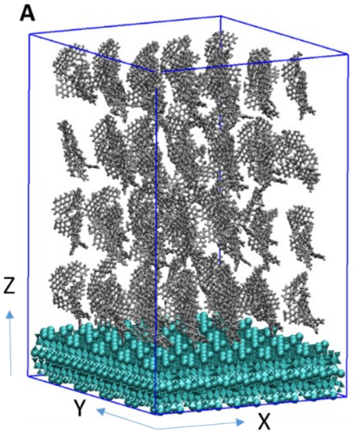

**Figure S1.** Initial configuration used to build a kerogen surface. Kerogen molecules and muscovite surface are shown in silver and cyan, respectively.

The kerogen molecular model shown in Fig. 2A (main text) was developed by Ungerer et al.[1] to reproduce the analytically-determined elemental and functional composition of over-mature kerogen, including the H/C, O/C, N/C, and S/C ratios, the average aromaticity, and the average size of the aromatic unit.[2] This model has chemical formula of $C_{175}H_{102}O_9N_4S_2$. In our previous papers[3-5] and this work, kerogen was simulated using the CVFF force field[6] (a LAMMPS[7] data file containing all force field parameters for the kerogen molecule can be found in our previous paper[4]). In our previous publications[3-5] porous structure of kerogen built is periodic in all directions. It is difficult to simulate water contact angle on kerogen surface using a periodic kerogen structure. In this work, we used a different approach utilizing the kerogen/muscovite interface to construct a kerogen surface that is periodic in the x and y directions, and non-periodic in the z direction.

In Fig. S1 we show a simulation snapshot representing the initial configuration used to build kerogen surface.  We first placed 60 kerogen molecules on top of a muscovite surface in a box with dimensions of 89.67x103.66x104.32 $Å^3$. The size of the muscovite substrate was 89.67x103.66x18.68 $Å^3$. Muscovite is a phyllosilicate mineral that has TOT structure: an Al octahedral sheet sandwiches in between two Si tetrahedral sheets.[8] In a Si tetrahedral sheet, an Al atom substitutes for one out of every four Si atoms that yields a negatively charged sheet. The negative charge is balanced by potassium ions in the interlayer. Muscovite was selected because it has similar structure with illite, common clay mineral found in shale gas reservoir.[9] In our simulation, muscovite was simulated by ClayFF force field.[10]

The kerogen molecules in the simulation system shown in Fig. S1 were initially mixed up in a NVT simulation in which temperature was reduced from 1000 K to 300 K in 100 ps with 1 fs time step. For this simulation, we only considered short-range Lennard-Jones (LJ) interaction with a cut-off distance of 5 Å, and the muscovite surface was kept rigid. In addition, to quickly obtain the desired kerogen density the simulation box was deformed every 100 steps so that the final box size in the z direction was 39 Å after 100 ps (the initial box size in z direction was 104.32 Å). The periodic boundary condition was applied in all directions for this and all other simulations in this work.

Next, the system was equilibrated in a NVT ensemble simulation for 100 ps.  The temperature was kept constant at 300 K for this simulation and for all simulations described below using the Nose-Hoover scheme.[11] During this simulation, the Lennard-Jones cutoff was 10 Å and the long-range electrostatic interactions were calculated using the PPPM (particle-particle-particle-mesh) solver.[12] All kerogen and muscovite atoms were free to move during the course of the simulation.

Interactions among un-like atoms were calculated using the Lorentz-Berthelot mixing rules $\varepsilon_{ij} = \sqrt{\varepsilon_{ii}\varepsilon_{jj}}$ and $\sigma_{ij} = (\sigma_{ii} + \sigma_{jj})/2$, where ε and σ are the depth of the potential energy well and the distance at which the inter-particle Lennard-Jones potential is zero, respectively. In the final step, the whole system was equilibrated in a NPT (constant number of atoms, pressure, and temperature) simulation for 2 ns. The pressuse (1 atm) was controlled in z direction using the Nose-Hoover scheme.[11, 13]

The final configuration of the simulation system is shown in Fig. 2B. The box size in the z direction is 41.90 Å including 18.68 Å of muscovite surface. The calculated kerogen density is 1.24 g/cm$^3$, which is in agreement with experimental data.[14] Note that we used LJ cut-off of 5 Å to initially mix up the kerogen molecules in the NVT simulation. If we used LJ cut-off of 10Å the kerogen molecules quickly aggregate and it becomes impossible to compress the kerogen structure to the constrained density of 1.24 g/cm$^3$. In the subsequent simulations, we used LJ cut-off of 10Å to make sure that interaction of a kerogen molecule with other molecules are correctly calculated. After removing the muscovite surface a kerogen/vacuum interface was obtained (Fig. 2C) and used in the simulations of contact angle and Poiseuille flow described below. This is the only kerogen surface created in this work. Note that for random network porous materials like our kerogen structure, the final configuration usually depends on the initial configuration and the method used to create it. Multiple porous structures are required to obtain reliable statistics for the results. In our previous work,[3] we created 9 kerogen samples from 9 initial configurations. The densities of kerogen samples varied from 1.172 g/cm$^3$ to 1.287 g/cm$^3$. The average density calculated from the 9 samples is 1.22±0.04 g/cm$^3$, which is consistent with experimental data of 1.28±0.3 g/cm$^3$.[14] In this work, our kerogen density is 1.24 g/cm$^3$, which is comparable with the calculated average density from 9 samples in our previous paper (1.22±0.04 g/cm$^3$) and also comparable with experimental result (1.28±0.3 g/cm$^3$).[14] Because our kerogen surface structure can reproduce the average kerogen properties we used it as an example to study kerogen wettability and fluid flow in nanopores.

## 2. Contact angle simulation

The wettability of kerogen was studied by performing MD simulations of 1100 water molecule droplets on the kerogen surface under different conditions. In Fig. S2A we report the initial configuration used to study the contact angle of pure water on kerogen surface. The initial box size was 89.67x103.66x100 Å$^3$. This simulation was carried out in a NVT ensemble. The result was discussed in Fig. 3A. The final configuration of this simulation (i.e., as shown in Fig. 3A) was then used in the simulation of the water droplet in $CO_2$ by adding $CO_2$ molecules into the system as shown in Fig. S2B. In Fig. S2C, we show the initial configuration to study the contact angle of the water droplet in $N_2$ or $CH_4$. Note that for the water drop in $CO_2$ simulation, when we use the same initial configuration as that for $N_2$ and $CH_4$ (Fig. S2C) we obtained the same result as when we use the initial configuration shown in Fig. S2B. For all contact angle simulations with gas, the simulations were performed in the NPT ensemble with $T = 300$ K and $P = 200$ atm (pressure was coupled in the direction perpendicular to the kerogen surface). The number of $CO_2$, $CH_4$ and $N_2$ molecules were 8524, 4757, and 4757, respectively. Note that $CO_2$ at 200 atm is supercritical and has higher density compared to that of $CH_4$ and $N_2$. To obtain approximately the same volume at the same pressure (to minimize the effect of system dimensions on the results) we used higher number of $CO_2$ molecules compared that of $CH_4$ and $N_2$.

Water molecules were simulated using the flexible SPC water model.[15] The $CH_4$ and $CO_2$ molecules were modeled by the TRaPPE force field.[16] In our previous research,[3] we compared the $CH_4$ gas adsorption onto kerogen using Grand Canonical Monte Carlo simulation with experimental data. The $CH_4$ molecule was simulated with TRaPPE force field and kerogen was modeled with CVFF force field. The comparison indicated that the gas adsorption data from molecular simulation is on the same order of magnitude, compared to the experimental data. In another study we compared the adsorption of $CO_2$ onto kerogen with that of $CH_4$. We used TRaPPE force field for both $CO_2$ and $CH_4$. The comparison suggested the preferential adsorption of $CO_2$ over $CH_4$, which agrees with the trend observed in actual measurement. In this work, we continue using TRaPPE force field[16] for both $CO_2$ and $CH_4$ and CVFF[6] for kerogen. In the TRaPPE force field, $CH_4$ molecules are described as united atoms and $CO_2$ is modeled as a 3-site rigid molecule. The rigidity of the $CO_2$ molecule was maintained by using the algorithm proposed by Kamberaj.[17] The $N_2$ molecules were simulated by implementing force field parameters used by Maddox et al.[18] The Lennard-Jones cutoff was 10 Å and the long-range electrostatic interactions were calculated using PPPM integration.[12] All contact angle simulations were performed for 10 ns.

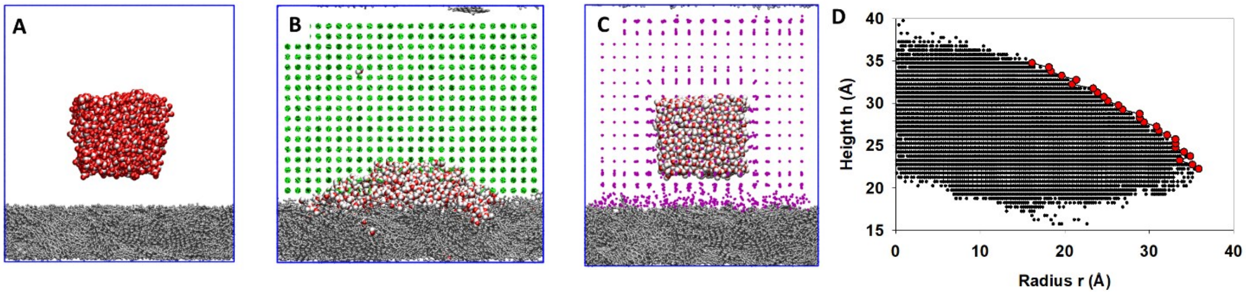

**Figure S2.** Initial configurations used to model contact angle of water droplet in vacuum (A), in $CO_2$ (B) and in $CH_4$ (C) on kerogen surface. The color code is similar to that in Fig.3. The droplet prolife used to calculate the contact angle (D). The contact angle was obtained by fitting the red data points in Fig. D using the function h=$Ar^2$+$Br$ +$C$, where h and r are the height and radius of the droplet, respectively; A, B, C are constants.

The last 6 ns of the contact angle simulation was divided into three blocks. The contact angle was calculated for each block to obtain the average and standard deviation as reported in the main text. The method implemented to estimate the contact angle from simulation trajectories was proposed by Giovambattista et al.[19] The z-axis passing through the center of mass of the drop and perpendicular to the solid surface was defined. The droplet was then divided into bins of 0.25 Å in the radius direction and 0.5 Å in the z direction to calculate the density profile. The typical density profile for the water droplet in vacuum on the kerogen surface is shown in Fig. S2D. The gas or vacuum/water interface was defined to be where the water density equals 20% of the bulk water density. The top 5 Å of the water molecules was excluded from the contact angle calculation [At the kerogen/water interface, we excluded the data that has a radius smaller than the largest radius in the droplet profile (see Fig. S2D)]. The remaining data points (red in Fig. S2D) were fitted using the equation h=$Ar^2$+$Br$ +$C$, where h and r are the height and radius of the droplet, respectively; $A$, $B$, and $C$ are the constants.

Note that the contact angle of a nanoscale spherical droplet[20] or of a periodic cylindrical droplet[21] depends on the droplet size. In the contact angle calculation, the determination of the water/gas and water/solid interfaces is also arbitrary. Therefore, the calculation of the contact angle using the nanoscale droplet is subject to some uncertainty, especially for highly hydrophilic surfaces. Alternatively, the contact angle can be calculated directly from Young' equation without explicitly simulating the droplet.[22] However the method to calculate the surface tension of the solid/fluid interface is not straightforward in MD simulation.[22] Because our work concerns with the general wetting properties and wetting trends under different conditions, we applied the most common method to perform the contact angle calculation.

## 3. Poiseuille flow simulation

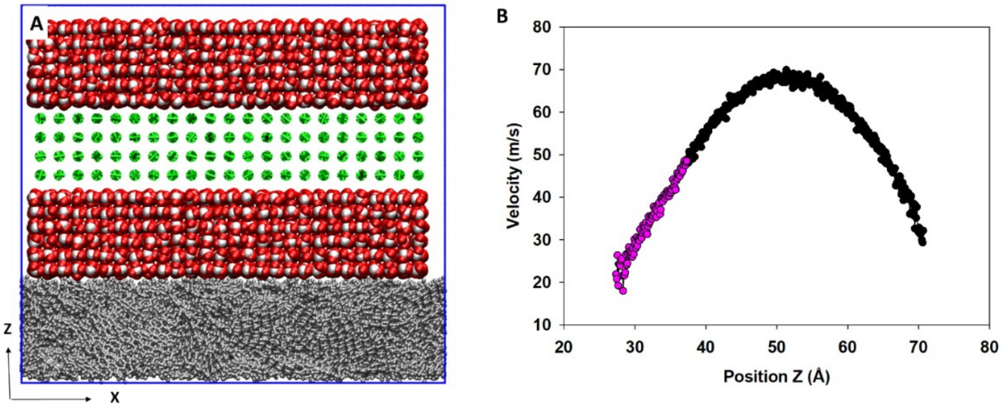

**Figure S3.** Initial configuration demonstrates water and $CO_2$ mixture confined in kerogen nanopore (the periodic boundary condition was applied in all directions) used in the flow simulation (A). The color code is the same as that in Fig. 1 (main text). The velocity profile of water (similar to that presented in Fig. 1C) in the kerogen nanochannel when steady state is obtained (B). The pink color represents the first 10Å data points from the interface that was used to fit the function $V=Az + B$ to calculate the slip length, where V is the velocity, z is the position, and A and B are constants.

In Fig. S3 we report the initial configuration used to study water flow with $CO_2$ or without $CO_2$ in the kerogen nanochannel. When the periodic boundary condition is applied in all directions we obtain a kerogen nanopore filled with pure water or with a mixture of water and $CO_2$. The initial box size was 89.67x103.66x80 Å$^3$. Before the flow simulation, an equilibrium MD simulation was carried out in a NPT simulation with temperature of 300K and pressure of 200 atm applied in the z direction for 10ns. All other simulation conditions were the same as those applied in the contact angle simulation. The number of water and $CO_2$ molecules in the nanopore are 10950 and 2100, respectively. During this simulation, $CO_2$ molecules eventually diffuse from the middle of the pore toward the kerogen surfaces and accumulate near kerogen/water interfaces as discussed in the main text.

The final configuration obtained from the equilibrium simulation above was used to initiate the non-equilibrium flow simulation. In the flow simulation, a body force (i.e., an acceleration of $3\times10^{-4}$ Kcal/Å.g or $\sim12.55\times10^{12}$ m/s$^2$) was added to all water molecules in the x direction. In MD simulation, the acceleration is on the order of $10^{11}$-$10^{12}$ m/s$^2$,[23, 24] so that the noise from the thermal motion can be avoided (with the limitation of the computational resources).[25] In our simulation the applied acceleration is slightly higher than that in the literature due to the surface roughness[26] and likely high confined pressure (200atm) in the z direction. The flow simulation was carried out for 20 ns in the NVT ensemble. Note that before conducting the flow simulation we carried out a NPT equilibrium simulation with pressure of 200 atm applied on the direction perpendicular to the kerogen surface. Therefore, in the flow simulation, we can assume that the pressure in the z direction is 200 atm. This pressure is similar to the confining pressure in the measurement of the permeability of fluid through rock using triaxial apparatus.[27] Similar MD simulation setup can be found in previous work.[28] During the flow simulation, a few atoms belonging to the kerogen surfaces were excluded from the integration of the equation of motion to keep the kerogen surface stationary (i.e., the velocity of kerogen surface is zero). All other atoms were free to move. In our previous work[5] we have shown that kerogen can expand its initial volume up to 11% in 200 atm $CO_2$ environment. Since the majority of kerogen atoms are free to move to some extent in the simulation presented in this work, we expect that the kerogen surface can deform. However, it is challenging to quantify the deformation of the kerogen surface because of the rough interface. The velocity and density profile of water in nanochannel shown in Fig. 1 were calculated after the flow reached steady state.

The velocity and slip length were calculated from the last 10 ns of the 20 ns flow simulation trajectories. The accuracy of the slip length calculation depends on the method used to fit the data points in the velocity profile presented in Fig. 1. For the slip length at planes A and B (see Fig. 1C) we used the data points at first 10 (i.e., shown in pink in Fig. S3B), 15, and 20 Å from the interface to fit with the function $V = AZ + B$, where V is the velocity, Z is the position, A and B are constants. The average slip length and standard deviation were calculated from three results obtained from this fitting procedure.

## 4. 1D-density profile of $CO_2$ with respect to kerogen atoms

The density profile of $CO_2$ shown in Fig. 1C presents an estimation for the relative position of $CO_2$ layers with respect to water and kerogen surface. Because the kerogen surface is rough, such density profile provides little information about the interaction of $CO_2$ with kerogen atoms. In Fig. S4 we report the density profile of carbon atom of $CO_2$ molecule and oxygen atom of water molecule as a function of shortest distance[29] to carbon and hydrogen atoms of kerogen to provide more information about the interaction of $CO_2$ and $H_2O$ with kerogen atoms. For example, for the $C_{CO2}$-$C_{kerogen}$ profile, the distances of a carbon atom of $CO_2$ molecule ($C_{CO2}$) to all carbon atoms of kerogen surface ($C_{kerogen}$) were calculated, and the shortest distance was recorded. The density prolife was then constructed by counting the number of $C_{CO2}$ as a function of shortest distance to $C_{kerogen}$. We only consider $C_{CO2}$ that is within 15Å from a kerogen atom. The density profile was then normalized by the total number of $C_{CO2}$ counted within 15Å from a kerogen atom.

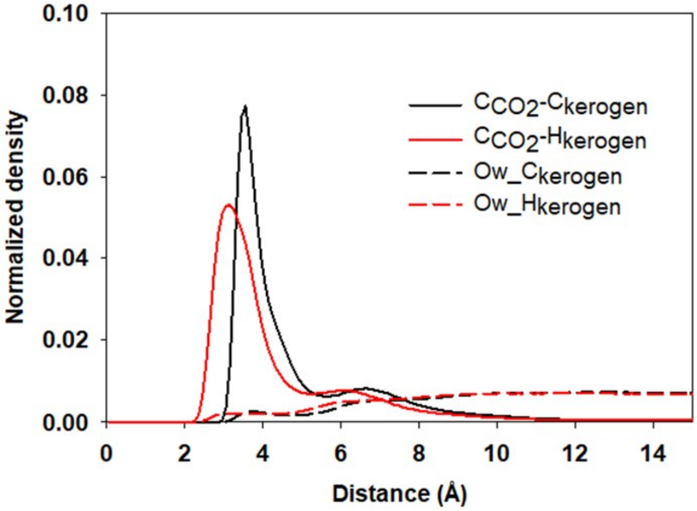

**Figure S4**. Normalized density profiles of carbon atom of $CO_2$ molecule and oxygen atom of water molecule with respect to carbon and hydrogen atoms of kerogen.

The density profile suggests that $C_{CO2}$ stays closer to the hydrogen atom of kerogen $H_{kerogen}$ than $C_{kerogen}$. The peaks around 3-4Å on the density of $C_{CO2}$ with respect to $H_{kerogen}$ and $C_{kerogen}$ are largely due to the accumulation of $CO_2$ layer near kerogen surface. Far away from kerogen atoms, the $C_{CO2}$ density vanishes. Compared to $C_{CO2}$, the density of water oxygen (Ow) with respect to kerogen atoms indicates that most of water molecules stay far away from kerogen atoms in the nanochannel.

## 5. Geometry, Lennard-Jones parameters $\varepsilon_i$ and $\sigma_i$, charge $q_i$ of $CO_2$, $CH_4$, $H_2O$, and muscovite simulated in this work.

| Atom | Geometry$^a$ | $\varepsilon_i$ (kcal/mol) | $\sigma_i$ (Å) | $q_i$ (e) |
|---|---|---|---|---|
| $C_{CO_2}$ | 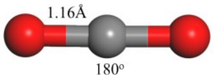 | 0.05365 | 2.80 | +0.70 |
| $O_{CO_2}$ | | 0.15697 | 3.05 | -0.35 |
| $O_w$ | 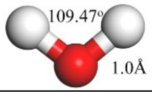 | 0.15539 | 3.16 | -0.82 |
| $H_w$ | | 0 | 0 | +0.41 |
| $CH_4$ | | 0.294076 | 3.73 | 0 |
| $Si_{st}$ | | $1.8405 \times 10^{-6}$ | 3.3019 | +2.1 |
| $Al_{ao}$ | | $1.3297 \times 10^{-6}$ | 4.2713 | +1.575 |
| $Al_{at}$ | | $1.8405 \times 10^{-6}$ | 3.3019 | +1.575 |
| $O_{obts}$ | | 0.1554 | 3.16 | 1.1688 |
| Oob | | 0.1554 | 3.16 | -1.05 |
| $O_{oh}$ | | 0.1554 | 3.16 | -0.95 |
| $H_{oh}$ | | 0 | 0 | +0.425 |
| $K^+$ | | 0.10 | 3.33 | +1 |

$Si_{st}$: tetrahedral silicon, $Al_{ao}$: octahedral aluminum, $Al_{at}$: tetrahedral aluminum, $O_{obts}$: bridging oxygen with tetrahedral substitution, Oob: bridging oxygen, $O_{oh}$: hydroxyl oxygen, $H_{oh}$: hydroxyl hydrogen

## References

1. P. Ungerer, J. Collell and M. Yiannourakou, *Energ Fuel*, 2015, **29**, 91-105.
2. S. R. Kelemen, M. Afeworki, M. L. Gorbaty, M. Sansone, P. J. Kwiatek, C. C. Walters, H. Freund, M. Siskin, A. E. Bence, D. J. Curry, M. Solum, R. J. Pugmire, M. Vandenbroucke, M. Leblond and F. Behar, *Energ Fuel*, 2007, **21**, 1548-1561.
3. T. A. Ho, L. J. Criscenti and Y. F. Wang, *Sci. Rep.*, 2016, **6**, 28053.
4. T. A. Ho, Y. Wang, Y. Xiong and L. J. Criscenti, *Fuel*, 2018, **220**, 1-7.
5. T. A. Ho, Y. Wang and L. J. Criscenti, *Phys. Chem. Chem. Phys.*, 2018, **20**, 12390-12395.
6. A. T. Hagler, S. Lifson and P. Dauber, *J. Am. Chem. Soc.*, 1979, **101**, 5122-5130.
7. S. Plimpton, *J. Comput. Phys.*, 1995, **117**, 1-19.
8. J. W. Wang, A. G. Kalinichev, R. J. Kirkpatrick and R. T. Cygan, *J. Phys. Chem. B*, 2005, **109**, 15893-15905.
9. T. A. Ho and A. Striolo, *AIChE J.*, 2015, **61**, 2993-2999.
10. R. T. Cygan, J. J. Liang and A. G. Kalinichev, *J. Phys. Chem. B*, 2004, **108**, 1255-1266.
11. S. Nose, *Mol. Phys.*, 1984, **52**, 255-268.

12. R. W. Hockney and J. W. Eastwood, *Computer simulation using particles*, Taylor & Francis Group, LLC., New York, 1988.
13. G. J. Martyna, D. J. Tobias and M. L. Klein, *J. Chem. Phys.*, 1994, **101**, 4177-4189.
14. A. Stankiewicz, N. Ionkina, B. Motherwell, B. W. Bennett, O. and M. Mastelerz, presented in part at the Paper presented at the Unconventional Resources Technology Conference, San Antonio, Texas, July 2015, 2015.
15. O. Teleman, B. Jonsson and S. Engstrom, *Mol. Phys.*, 1987, **60**, 193-203.
16. J. J. Potoff and J. I. Siepmann, *AIChE J.*, 2001, **47**, 1676-1682.
17. H. Kamberaj, R. J. Low and M. P. Neal, *J. Chem. Phys.*, 2005, **122**, 224114
18. M. W. Maddox, J. P. Olivier and K. E. Gubbins, *Langmuir*, 1997, **13**, 1737-1745.
19. N. Giovambattista, P. G. Debenedetti and P. J. Rossky, *J. Phys. Chem. B*, 2007, **111**, 9581-9587.
20. J. G. Zhang, F. Leroy and F. Muller-Plathe, *Phys. Rev. Lett.*, 2014, **113**.
21. G. Scocchi, D. Sergi, C. D'Angelo and A. Ortona, *Phys. Rev. E*, 2011, **84**.
22. H. Jiang, F. Müller-Plathe and A. Z. Panagiotopoulos, *The Journal of Chemical Physics*, 2017, **147**, 084708.
23. Z. Q. Zhang, L. S. Yuan, Z. Liu, G. G. Cheng, H. F. Ye and J. N. Ding, *Comp Mater Sci*, 2018, **145**, 184-190.
24. S. K. Kannam, B. D. Todd, J. S. Hansen and P. J. Daivis, *J. Chem. Phys.*, 2012, **136**.
25. E. Lauga, M. P. Brenner and H. A. Stone, *Handbook of Experimental Fluid Dynamics*, Springer, New York, 2007.
26. B. Liu, R. B. Wu, A. W. K. Law, X. Q. Feng, L. C. Bai and K. Zhou, *Sci. Rep.*, 2016, **6**.
27. J. F. Van Stappen, R. Meftah, M. A. Boone, T. Bultreys, T. De Kock, B. K. Blykers, K. Senger, S. Olaussen and V. Cnudde, *Environ. Sci. Technol.*, 2018, **52**, 4546-4554.
28. C. Gattinoni, D. M. Heyes, C. D. Lorenz and D. Dini, *Phys. Rev. E*, 2013, **88**.
29. T. A. Ho, J. A. Greathous, A. S. Lee and L. J. Criscenti, *Langmuir*, 2018, **34**, 5926-5934.